INTERNATIONAL JOURNAL FOR NUMERICAL METHODS IN FLUIDS
Int. J. Numer. Meth. Fluids 2017; **83**:664–678
Published online 17 August 2016 in Wiley Online Library (wileyonlinelibrary.com). DOI: 10.1002/fld.4286

Study of a collocated Lagrange-remap scheme for multi-material flows adapted to HPC

Jean-Philippe Braeunig*,† and Bastien Chaudet

CEA/DAM/DIF F-91297 Arpajon, France

SUMMARY

This paper describes a collocated numerical scheme for multi-material compressible Euler equations, which attempts to suit to parallel computing constraints. Its main features are conservativity of mass, momentum, total energy and entropy production, and second order in time and space. In the context of a Eulerian Lagrange-remap scheme on planar geometry and for rectangular meshes, we propose and compare remapping schemes using a finite volume framework. We consider directional splitting or fully multi-dimensional remaps, and we focus on a definition of the so-called corner fluxes. We also address the issue of the internal energy behavior when using a conservative total energy remap. It can be perturbed by the duality between kinetic energy obtained through the conservative momentum remap or implicitly through the total energy remap. Therefore, we propose a kinetic energy flux that improves the internal energy remap results in this context. Copyright © 2016 John Wiley & Sons, Ltd.

Received 23 February 2016; Accepted 18 July 2016

KEY WORDS: Eulerian; finite volume; Lagrangian; collocation; compressible flow; free surface; parallelization; thermodynamics

1. INTRODUCTION

The goal of this study is to propose a multi-material Eulerian scheme solving the compressible Eulerian equations suitable for multi-physics HPC (High Performance Computing) hydrocodes. The methods presented in this paper are developed in the SHY (Scalable HYdrodynamics) code platform dedicated to research in HPC (High Performance Computing) and numerics at CEA DIF (French Atomic Energy Commission). As conduct lines for the design of this scheme, we obviously anticipate that meshes will be refined thanks to the increase of computational power, thus, the scheme should be robust and at least second order in time and space. Moreover, the scheme should be conservative of mass, momentum, total energy and entropy to converge to the right solution. For the sake of making easy multi-physics extension of the scheme, we have chosen to investigate Lagrange-remap schemes. They consist during a one-time step in a Lagrangian phase in which quantities evolve on a moving grid, then, they are remapped on the initial mesh, like in the Arbitrary Lagrangian Eulerian (ALE) framework. Another constraint is to allow a proper scalability of the code when using supercomputers with many cores, thus, the number of MPI (Message Passing Interface) parallel synchronizations in the algorithm should be limited, and remap should be generic to allow Open Multi-Processing parallel loops and vectorization.

We choose a collocated Lagrangian scheme [1–4] because it provides conservativity, robustness, and simple data structures because all quantities are located at cell centers. They are thoroughly investigated these days, and we choose the EUCCLHYD Lagrangian scheme [2, 17, 18] as the basis for this Eulerian scheme, because it has good properties and has existing extensions to multi-physics like elasto-plastic flows [5], cylindrical geometries [6], coupling with a diffusion scheme [7], and

*Correspondence to: Jean-Philippe Braeunig, CEA/DAM/DIF F-91297 Arpajon, France.
†E-mail: jpbraeunig@yahoo.fr

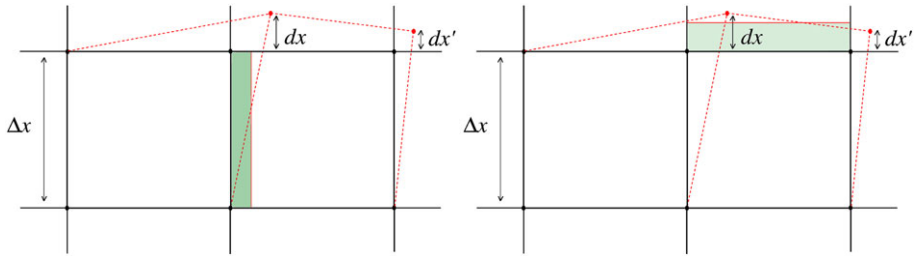

Figure 1. Alternate Directions steps producing a corner flux.

sharp interface capturing [8]. A collocated conservative remap of mass, momentum, and total energy is required to keep the benefit of a conservative Lagrangian phase. It is well known that such a remap may lead to internal energy issues when using second order reconstruction of the variables because kinetic energy is remapped ambiguously between the momentum remap with linear reconstruction of velocity and the total energy remap in which implicitly kinetic energy (velocity square) is linearly reconstructed. We then propose a kinetic energy flux, which improves the behavior of the internal energy remap through the total energy remap.

When restricting to Cartesian orthogonal meshes, Alternate Directions (AD) remap by performing monodimensional successive remap at each time step is popular to easily obtain multi-dimensional Eulerian schemes. Results are good for many flows, including when using multi-material methods with VOF-PLIC (Volume Of Fluid-Piecewise Linear Interface Capturing) interface reconstruction [9, 10]. One reason is that the directional splitting implicitly produces a diagonal flux, because successive monodimensional X then Y (or Y then X) remap makes a cell information reach its diagonal right-top neighbor. For instance in one time step, see Figure 1. The flux value in diagonal direction in the mesh is usually called 'corner flux', but it is not a classical finite volume flux because a corner has no area to go through. However, it is known that this flux is crucial for shape advection in a grid especially when using interface reconstruction, and it appears naturally in Lagrange-remap schemes as we will see. In AD remap, this flux is not accurately computed but gives astonishingly good results at least on simple cases. One major drawback about parallel computational performance of the AD remap is that a synchronization is necessary at the end of each monodimensional remap, thus, three in 3D. Therefore, the purpose of this study is to propose a direct multi-dimensional remap where only one parallel synchronization is necessary, using the same basic functions as the multi-material AD scheme (polygon collection and intersection) [11]. Of course, we want to obtain a good accuracy of the scheme, at least compared with AD remap, which will be our reference. It is well known that a direct multi-dimensional remap, meaning the naive finite volume normal to faces flux discretization, does not give good results. Explicit corner fluxes have then to be defined to recover close results from those of AD remap. We propose a simple Lagrangian cell representation with corner fluxes and normal fluxes through faces, which is inspired among others by *Leveque* [12] and *Rider and Kothe* [11].

This study is restricted to 2D Cartesian orthogonal meshes in planar geometry and multi-material flows with two materials (sharp interface). In Section 2, we describe the Eulerian multi-material collocated scheme, with the Lagrangian phase and different remaps, which results will be compared. In Section 3, we propose a second order collocated remap scheme, which has an improved internal energy behavior when using a momentum and total energy conservative remap.

2. COLLOCATED LAGRANGE-REMAP SCHEME FEATURES

2.1. Lagrangian phase

We use here the collocated Lagrangian scheme EUCCLHYD (*P.-H. Maire et al, 2007* [2]), but it could be as well GLACE (*Després et al, 2005* [13]), to solve the Euler equations in their Lagrangian form:

DOI: 10.1002/fld

$$\begin{cases} \dfrac{d}{dt}\displaystyle\int_{\Omega(t)} 1 dV & = \displaystyle\int_{\Omega(t)} (\vec{\nabla}.\vec{u})(x.t) dV \\ \dfrac{d\vec{x}(t)}{dt} & = \vec{u}(x,t) \\ \dfrac{d}{dt}\displaystyle\int_{\Omega(t)} \rho(x,t) dV & = 0 \\ \dfrac{d}{dt}\displaystyle\int_{\Omega(t)} \rho(x,t)\vec{u}(x,t) dV & = -\displaystyle\int_{\Omega(t)} \vec{\nabla} P(x,t) dV \\ \dfrac{d}{dt}\displaystyle\int_{\Omega(t)} \rho(x,t)E(x,t) dV & = -\displaystyle\int_{\Omega(t)} \vec{\nabla}.(P(x,t)\vec{u})(x,t) dV \\ P(x,t) & = EOS(\rho(x,t), e(x,t)) \end{cases}$$

with ρ the density, P the pressure, E the specific total energy, $e = E - |\vec{u}|^2/2$ the specific internal energy, $\vec{u}$ the velocity on volume $\Omega(t)$, and EOS an equation of state.

The multi-material collocated Lagrange scheme follows *Galera et al's* work for multi-material ALE [8]. We will not recall all details of this work but the main steps of this Lagrangian phase:

1. Solving acoustic Godunov Riemann problems at nodes, to obtain node velocities and half edges pressures with the following constraints:
   - volume, momentum, and total energy conservation,
   - entropy dissipation through acoustic Riemann problems.
2. Edge fluxes are computed with node velocities and half edges pressures, then each node position $\vec{x}$, cell volume Vol, velocity $\vec{u}$, and specific total energy E are updated.
3. In a mixed cell i containing several materials α, we use the following subcell model:
   - velocity is the same for all materials α of cell i, thus $u_\alpha = u_i$,
   - materials' densities evolve considering iso-deformation of all materials, that is, volume fractions remain the same between time t^n and t^{lag}:

$$f_\alpha^{lag} = Vol_\alpha^{lag}/Vol_i^{lag} = f_\alpha^n = Vol_\alpha^n/Vol_i^n,$$

   - each material has its own equation of state to obtain the partial pressure $p_\alpha = EOS_\alpha(\rho_\alpha, e_\alpha)$,
   - a mixture pressure is defined to compute EUCCLHYD's fluxes, which is a volume average of materials pressures p_α:

$$\overline{p}_i = \sum f_\alpha p_\alpha,$$

   - specific internal energy for each material e_α is computed assuming the same specific entropy dissipation rate for each material equal to the cell i mixture specific entropy dissipation rate:

$$(T d_t s)_i = d_t e_i + \overline{p}_i^n d_t Vol_i/m_i = d_t e_\alpha + f_\alpha^n p_\alpha^n d_t Vol_i/m_\alpha$$

Second order in space is obtained by a multi-dimensional MUSCL (Monotonic Upstream-Centered Scheme for Conservation Laws) linear reconstruction at nodes of cell centered variables $Q = (u, v, p)$, to feed the Riemann problems at nodes. Second order in time is obtained with a predictor-corrector or Runge–Kutta 2 integration. These techniques to get higher order differs from *Maire et al*'s approach [6, 8].

2.2. Alternate Directions remap

The Lagrangian step is done, thus, the mesh nodes positions x^{lag}, the volumes Vol^{lag}, the masses $m^{lag} = m^n$, the velocities u^{lag}, and the total energies E^{lag} are known at cell centers. At each iteration n in 2D, two steps are performed: a 1D remap in direction x, and this result is remapped 1D in

DOI: 10.1002/fld

direction y. Directions x and y are alternated at each iteration n. The remap steps for direction x are the following:

1. $V\,ol_i^{lagx}$ is the 1D approximation of the Lagrangian cell volume $V\,ol^{lag}$, with right r and left l faces boundaries of the cell i in direction x :

$$V\,ol_i^{lagx} = V\,ol_i^n + dV\,ol_r - dV\,ol_l,$$
$$\rho_i^{lagx} = \frac{m_i^{lag}}{V\,ol_i^{lagx}},$$

2. Remap of mass, momentum, and total energy:

$$\begin{aligned} m_i^{remap} &= m_i^{lagx} - \rho_r^{lagx\,o2} dV\,ol_r + \rho_l^{lagx\,o2} dV\,ol_l \\ m_i^{remap} u_i^{remap} &= m_i^{lagx} u_i^{lagx} - \rho_r^{lagx\,o2} u_r^{lag\,o2} dV\,ol_r + \rho_l^{lagx\,o2} u_l^{lag\,o2} dV\,ol_l \\ m_i^{remap} E_i^{remap} &= m_i^{lagx} E_i^{lagx} - \rho_r^{lagx\,o2} E_r^{lag\,o2} dV\,ol_r + \rho_l^{lagx\,o2} E_l^{lag\,o2} dV\,ol_l \end{aligned}$$

with the Lagrangian A_i^{lagx} and the remapped A_i^{remap} values in cell i, the second order limited linear reconstruction of density $\rho_f^{lagx\,o2}$, normal velocity $u_f^{lagx\,o2}$, total energy $E_f^{lagx\,o2}$ at faces $f = \{r, l\}$. The 1D volume displacement through face f is computed according to the averaged 1D x displacements of nodes: $dV\,ol_f = \Delta t\ \Delta y_f^n (x_{fp1}^{lag} + x_{fp2}^{lag} - x_{fp1}^n - x_{fp2}^n)/2$, with nodes $fp1$ and $fp2$ belonging to face f and $\Delta y_f^n = |y_{fp1}^n - y_{fp2}^n|$.

The multi-material extension of this scheme follows *Youngs* [10] algorithm. The interface is positioned in the 1D Lagrangian volume $V\,ol_i^{lagx}$ with constraints of conserving the volume fraction in cell i and defining an interface normal, which direction is computed with a discrete volume fraction gradient $\vec{n} = -\nabla f^n / \|\nabla f^n\|$ according to the neighbor cell values of f at time t^n. Volume fluxes $dV\,ol_f^\alpha$ for each material α are computed according to the geometric intersection between the positioned interface in the donor cell and the total volume flux $dV\,ol_f$. Associated quantities ρ_f^α, E_f^α are simply the values for material α in the donor cell. We recall that the velocity is the same for all materials in cell i, thus, it is remapped according to the cells total mass.

2.3. Direct multi-dimensional remap

At each iteration n, a volume displacement is computed through each faces and corners:

1. $V\,ol_i^{lagCF}$ is the multi-dimensional approximation of the Lagrangian cell volume $V\,ol_i^{lag}$, with f faces and p corners of cell i:

$$V\,ol_i^{lagCF} = Vol_i^n + \sum_{faces} dV\,ol_f + \sum_{corners} dV\,ol_p,$$
$$\rho^{lagCF} = \frac{m^n}{V\,ol^{lagCF}}$$

2. Remap of Lagrangian variables

$$\begin{aligned} m_i^{remap} &= m_i^{lag} + \sum_{faces} \rho_f^{lagCF\,o2} dV\,ol_f + \sum_{corners} \rho_p^{lagCF\,o2} dV\,ol_p \\ m_i^{remap} u_i^{remap} &= m_i^{lag} u_i^{lag} + \sum_{faces} \rho_f^{lagCF\,o2} u_f^{lag\,o2} dV\,ol_f \\ &\quad + \sum_{corners} \rho_p^{lagCF\,o2} u_p^{lag\,o2} dV\,ol_p \\ m_i^{remap} E_i^{remap} &= m_i^{lag} E_i^{lag} + \sum_{faces} \rho_f^{lagCF\,o2} E_f^{lag\,o2} dV\,ol_f \\ &\quad + \sum_{corners} \rho_p^{lagCF\,o2} E_p^{lag\,o2} dV\,ol_p \end{aligned}$$

DOI: 10.1002/fld

The volume displacement $dV\,ol_p$ at corner p is the rectangle defined by points $\mathbf{x}_p^n$ and $\mathbf{x}_p^{lag}$, with edges parallel to the axis, see Figure 2. The volume $dV\,ol_f$ is the exact integration of the Lagrangian face normal displacement with respect to its initial position (Eulerian grid), excluding the part overlapping corner fluxes $dV\,ol_p$. For instance with a linear profile for the face normal displacement $y(s)$ such that $y(x_p^{lag}) = y_p^{lag} - y_p^n$ with both corners $p = \{p1, p2\}$ and curvilinear abscissa s belonging to face f, it reads:

$$dV\,ol_f = \int_{x_1}^{x_2} y(s)ds = (x_2 - x_1)\frac{y(x_2) + y(x_1)}{2},$$

with if $x_{p1}^n < x_{p2}^n$: $x_1 = \max(x_{p1}^n, x_{p1}^{lag})$ and $x_2 = \min(x_{p2}^n, x_{p2}^{lag})$.

At face f, we use a 1D second order limited linear reconstruction, as for AD remap, of density $\rho_f^{lagCF\ o2}$, velocity $u_f^{lagCF\ o2}$, and specific total energy $E_f^{lagCF\ o2}$.

At corner p, reconstruction of these quantities may be carried out with different choices for quantity $Q = \{\rho, \mathbf{u}, E\}$:

- Upwinding at corners, as *Leveque* in [12]: for instance, if $\mathbf{u}_p \cdot \mathbf{e}_x > 0$ and $\mathbf{u}_p \cdot \mathbf{e}_y > 0$, we decentrate the value donor cell, here the bottom-left bl neighbor cell of p:

$$Q_p^{lag\ upw} = Q_{bl}^{lag}$$

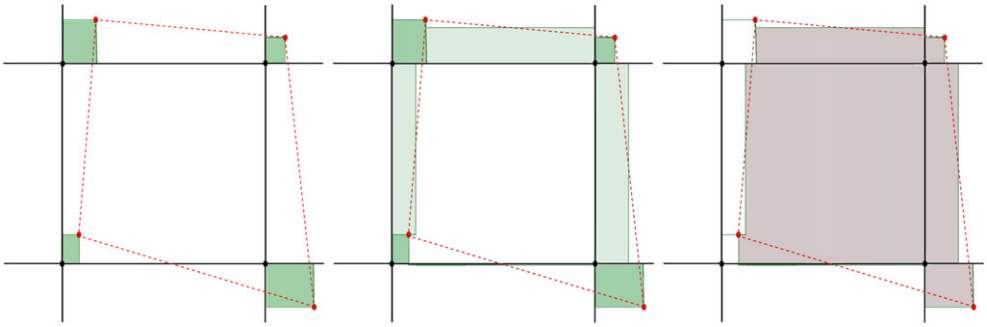

Figure 2. Construction of the Lagrangian cell approximation with corner fluxes, from the Lagrangian cell in red.

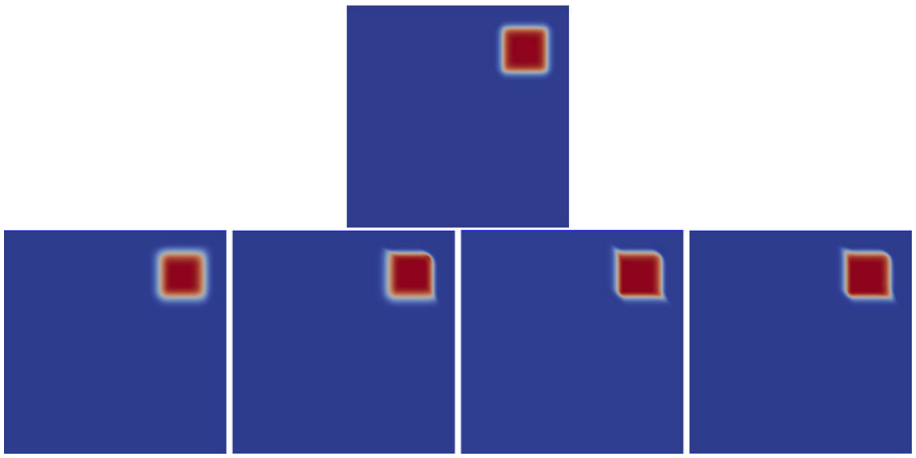

Figure 3. Alternate Directions at top, corner's value reconstruction at bottom, from left to right: upwind, diagonal average, xy gradients addition, diagonal gradient. Limited diagonal reconstruction at corners gives the closest result from the Alternate Directions remap.

DOI: 10.1002/fld

- Average between cell i and the neighbor cell in diagonal i_d with respect to p is as follows:

$$Q_p^{lag\,o2,\,avg} = \frac{1}{2}\left(Q_i^{lag} + Q_{i_d}^{lag}\right)$$

- Gradients addition: for instance, if $\mathbf{u}_p \cdot \mathbf{e}_x > 0$ and $\mathbf{u}_p \cdot \mathbf{e}_y > 0$, we use bottom fb and left fl faces limited gradients as follows:

$$Q_p^{lag\,o2,\,xy} = Q_{bl}^{lag} + \left(\frac{\partial Q^{lag}}{\partial x}\right)_{fb} \frac{\Delta x^{lag}}{2} + \left(\frac{\partial Q^{lag}}{\partial y}\right)_{fl} \frac{\Delta y^{lag}}{2}$$

- Diagonal gradient: for instance, if $\mathbf{u}_p \cdot \mathbf{e}_x > 0$ and $\mathbf{u}_p \cdot \mathbf{e}_y > 0$, we compute a gradient in the bottom-left bl donor cell in diagonal direction $\mathbf{v}$ by linear limited reconstruction as follows:

$$Q_p^{lag\,o2,\,diag} = Q_{bl}^{lag} + \left(D_{\mathbf{v}}\, Q^{lag}\right)_{bl} \frac{1}{2}\sqrt{(\Delta x^{lag})^2 + (\Delta y^{lag})^2}$$

We can observe in Figure 3 the results of the advection of a square shape of the density profile with velocity $(u, v) = (5, 5)$. Notice that for a linear advection test, there is no error in the volume reconstruction that is a square, when using the Direct remap with corner fluxes. The error is only coming from the variables reconstruction, and the choice about it at corners does have an importance, even

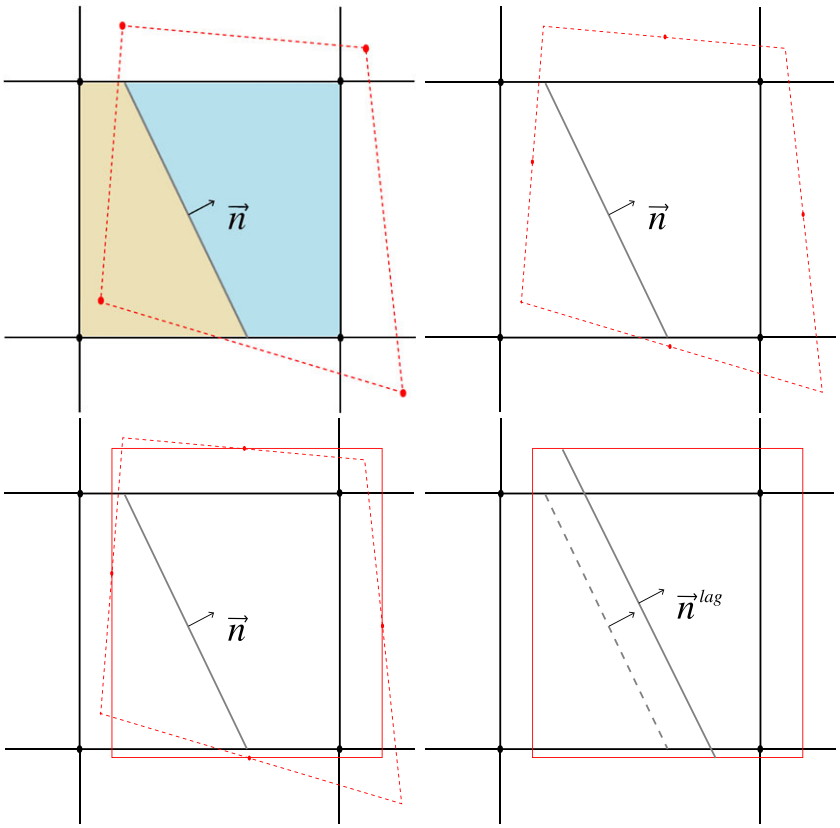

Figure 4. Interface positioning on a rectangular approximation of the Lagrangian cell.

DOI: 10.1002/fld

if corner volume fluxes are of smaller order than at faces. Upwind is order one, and numerical diffusion is visible compared with AD remap. The diagonal average is second order accurate, but gives symmetry breakings and spurious oscillations. Gradients addition deforms the shape, diagonal gradient also but a little less. We choose to run all test cases with diagonal gradient reconstruction at corners, knowing this default on this test case. Our opinion is that a multi-dimensional reconstruction is required to recover the same isotropy than with AD remap, which shows a very good result here. However, a shape without parallel edges to the axis, as this square shape, should show less artificial deformations.

The multi-material extension of this scheme is performed by defining a volume in which the material interface is positioned according to the volume fractions and the interface normal approximation, that is, the discrete gradient $n = -\nabla f^n / \|\nabla f^n\|$ like Youngs [10]. Because the multi-dimensional representation of the Lagrangian volume with corner fluxes $V\,ol_i^{lagCF}$ makes the interface positioning too complex, we have chosen to define a simple rectangular approximation of the Lagrangian cell, which edges are parallel to the axis and pass at the middle of the Lagrangian edges $V\,ol_i^{lag}$, see Figure 4. We then compute the interface position through a line equation in this rectangle, and we perform its intersection with faces $dV\,ol_f$ and corners $dV\,ol_p$ fluxes to obtain the materials α fluxes $dV\,ol_f^{\alpha}$ and $dV\,ol_p^{\alpha}$, see Figure 5.

2.4. *Comparison of Alternate Directions versus Direct Remap*

2.4.1. Rationale. Let us begin with an analytic illustration of the multi-dimensional remap accuracy, the one presented in section 2.3, on a simple situation in which only one node of a cell moves

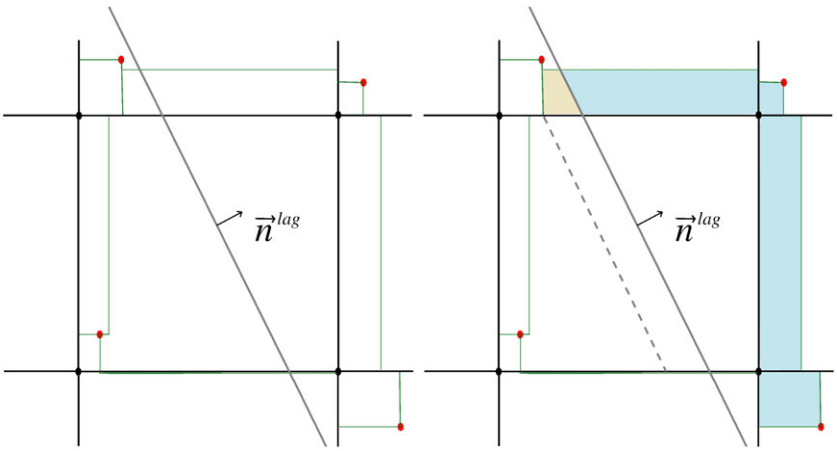

Figure 5. Multi-material fluxes computation by geometric intersection.

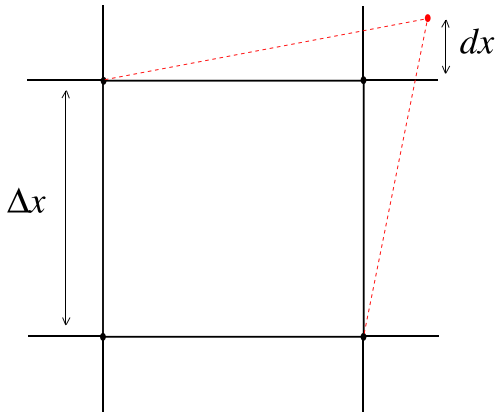

Figure 6. One node Lagrangian displacement with $\Delta t\ \vec{u} = (dx, dx)$, with $\varepsilon = dx/\Delta x$.

DOI: 10.1002/fld

with displacement $\Delta t\ \vec{u} = (dx, dx)$, see Figure 6. We normalize the approximated Lagrangian volume value $V\ ol^{lag}_{approx}$ with the non-deformed cell value Δx^2 and the displacement $\varepsilon = dx/\Delta x$. We can compare the exact Lagrangian cell volume with its approximation by each type of remap with $V\ ol^{lag}_{approx}/(\Delta x)^2$ function of $\varepsilon = dx/\Delta x$:

- Exact : $1 + \varepsilon$
- Direct without corner fluxes: $1 + \varepsilon$
- AD: $1 + \varepsilon + \varepsilon^2/4$
- Rectangular approximation: $1 + \varepsilon + \varepsilon^2/4$
- Direct with corner fluxes : $1 + \varepsilon + \varepsilon^3 + o(\varepsilon^3)$

It appears, see Figure 7, that the multi-dimensional reconstruction without corner fluxes 'Direct' gives the exact volume $1 + \varepsilon$, but the shape is far from the exact one and no information go through the moving node in the diagonal direction. AD and rectangular approximation "Rectangular", see Figure 4, give the same volume, with a first order error $\varepsilon^2/4$ compared with the exact value $1+\varepsilon$, but the shapes are different between these two remaps, and thus, the associated remap volume fluxes. The multi-dimensional Direct remap with corner fluxes gives a second order error ε^3 compared with the exact value $1 + \varepsilon$, which proves that this Lagrangian volume representation is more accurate than AD remap.

2.4.2. Numerical results. **Advection:** We will here compare the results for a square shape advection test case with and without interface reconstruction. It consists in the linear advection and return to initial position with velocity $\mathbf{u} = (5; 5)\,\mathrm{m\ s^{-1}}$. Different meshes are used 50×50, 100×100, 200×200, 400×400 to verify the methods.

Without interface capturing, we can observe in Figure 8 a strong mesh imprinting on the square shape when using Direct remap without corner fluxes. Result using AD show a good isotropy of numerical diffusion, while Direct remap with corner fluxes still show a small mesh imprinting. With

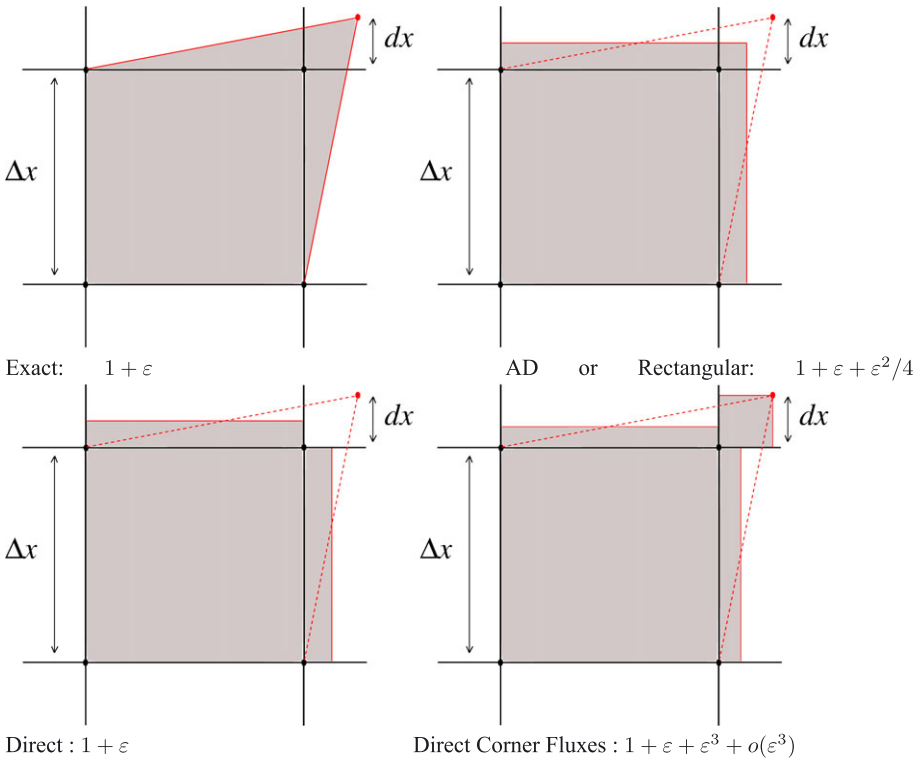

Figure 7. Comparison of Lagrangian volume geometry approximation for each remap (red) compared with the exact Lagrangian volume (dashed red).

DOI: 10.1002/fld

interface capturing, we can observe in Figure 9 that the square shape is deformed when using Direct remap without corner fluxes. Results using AD or Direct with corner fluxes remaps are similar, and the shape is being well preserved except the corners that are smoothed. One can compute the error on the volume fractions f compared with the exact solution for all meshes, see Figure 10, and it confirms that the Direct remap without corner flux is less accurate than both AD and Direct with

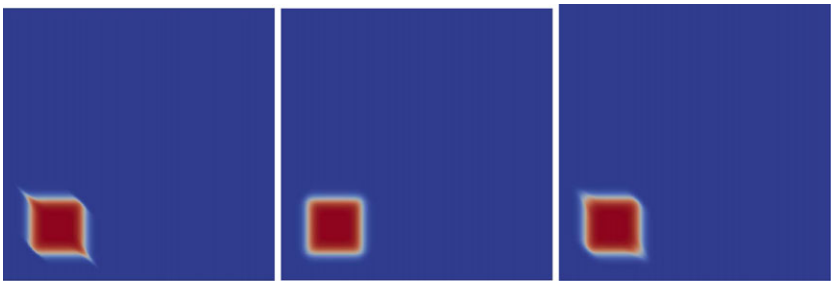

Figure 8. Advection of a square without interface reconstruction using different remaps: Direct without corner fluxes, Alternate Directions, Direct with corner fluxes with the mesh 100×100.

Figure 9. Advection of a square with interface reconstruction using different remaps: Direct without corner fluxes, Alternate Directions, Direct with corner fluxes with the mesh 100×100.

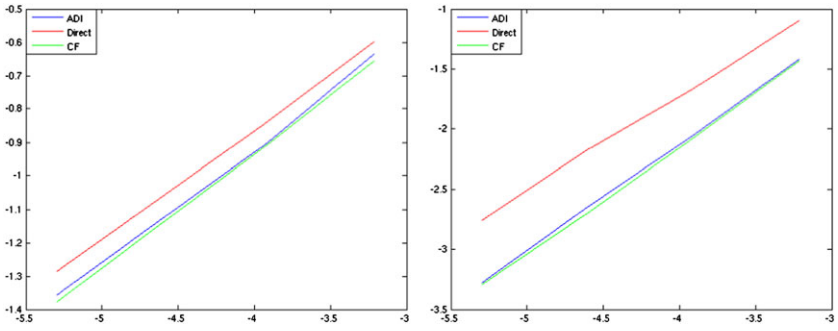

Figure 10. Left side without interface reconstruction, right side with it: $\log \parallel f_1^{final} - f_1^0 \parallel_{L^2}$ function of $\log(\Delta x)$. Alternate Directions 'ADI' and Direct with corner fluxes 'CF' remap show a similar behavior, with lower error than Direct without corner flux 'Direct' remap.

Table I. Data Haas–Sturtevant shock bubble Air-He interaction.

Initial state	Left air state (shock)	Right air state	Bubble
Density ρ (k gm^3)	1.376363	1	0.18187
Velocity $\mathbf{u}.\mathbf{e}_x$ (m s^{-1})	124.824	0	0
Pressure p (Pa)	$1.5698\ 10^5$	10^5	10^5
Gamma γ	1.4	1.4	1.66

DOI: 10.1002/fld

corner fluxes, the two last showing a similar behavior. The convergence rate is close to 0.4 without interface reconstruction and 0.9 with it, which means not much because the square shape is singular at corners, and the volume fraction is discontinuous at the interface.

Haas–Sturtevant shock bubble Air-He interaction: This 2D planar benchmark [14, 15] consists in the interaction between a shock in air and a cylindrical bubble of helium of radius 2.25 cm. We use the interface reconstruction between air and helium. It happens large deformations of the interface and a large advection of the bubble, thus, the remap is strongly tested as the symmetry preservation, because we compute the whole cylindrical bubble geometry. The mesh is 1000×90 for the domain $[0, 1000]\times[0, 9]$ cm. Final time is $t = 1$ ms. Initial values and γ for both perfect gases are given in Table I.

In Figure 11, we compare results using AD and Direct with corner fluxes remaps. The shapes are strikingly close, with the head of the mushroom position showing a difference less that one cell.

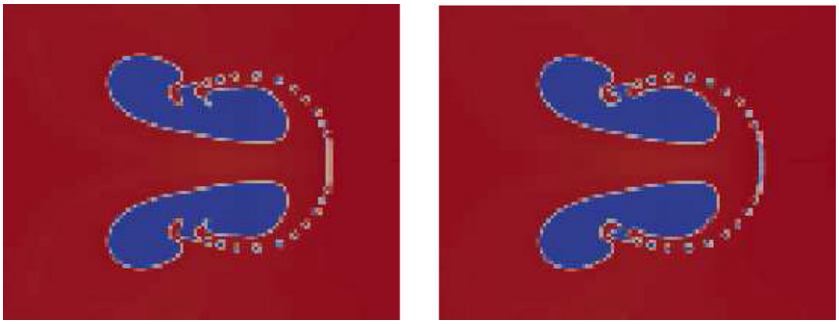

Figure 11. Volume fraction at final state, $t = 1$ ms. Alternate Directions at left side, Direct corner fluxes at the right side.

Table II. Data droplet impact on a thin film.

Initial state	Air	Wall	Drop
Density ρ (kg m^3)	1.29	1000	1000
Velocity $\mathbf{u}.\mathbf{e}_x$ (m s^{-1})	-1000	0	-1000
Pressure p (Pa)	10^5	10^5	10^5
Gamma γ	1.4	7	7
Pi π (Pa)	0	$2.1\,10^9$	$2.1\,10^9$

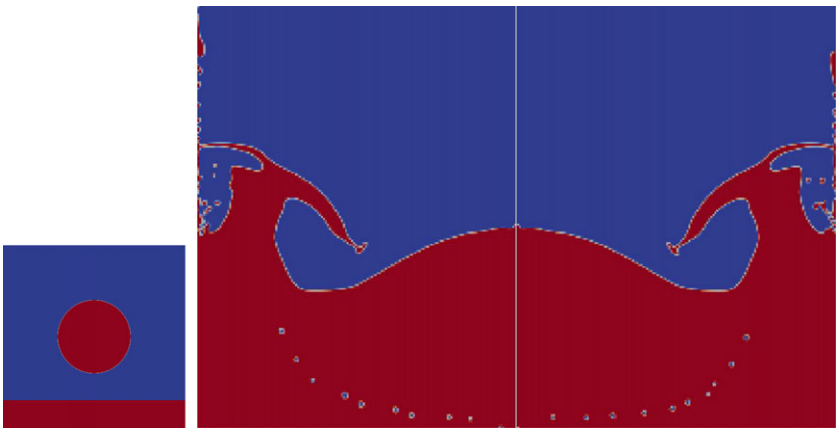

Figure 12. Volume fraction at initial state, $t = 0$s and $t = 6\mu s$. Alternate Direction at left side , Direct with corner fluxes at right side.

DOI: 10.1002/fld

Droplet impact on a thin film: a cylindrical water droplet is traveling into air and impacts a thin film of water [16]. The interface is between water and air, and the droplet interface and the film interface merges after the impact. This benchmark strongly tests the robustness of the whole scheme, because we use a stiffened gas equation of state for water and a perfect gas for air. The mesh is 320×160 for the domain $[0,10]\times[0,5]$ cm. We simulate only half the geometry using symmetry. Initial values and parameters for equations of state $p=(\gamma-1)\rho e-\pi$ are given in Table II.

In Figure 12, we compare results using AD and Direct with corner fluxes remaps. Again, the shapes are strikingly close, even for air droplets trapped during the impact. This comparison shows a great robustness of the method and a quite equivalent behavior between both remaps.

3. COLLOCATED REMAP SCHEME ISSUE ABOUT INTERNAL ENERGY

3.1. Total energy remap modification

The scheme described in this paper addresses a conservative remap in mass, momentum, and total energy, by a finite volume multi-dimensional flux remap. It is well known that total energy remap can produce under/overshoots in internal energy. We will here exhibit the process leading to this default and propose a conservative way to reduce it. The remap phase is achieved by using a flux scheme, thus is fully conservative:

$$\begin{cases} Vol_i &= Vol_i^{lag}+\sum_{cf} dVol_{cf} \\ m_i &= m_i^{lag}+\sum_{cf} dm_{cf} \\ u_i &= \left(u_i^{lag}m_i^{lag}+\sum_{cf} dqu_{cf}\right)/m_i \\ v_i &= \left(v_i^{lag}m_i^{lag}+\sum_{cf} dqv_{cf}\right)/m_i \\ E_i &= \left(E_i^{lag}m_i^{lag}+\sum_{cf} dmE_{cf}\right)/m_i \\ e_i &= E_i-(u_i)^2/2+(v_i)^2/2 \end{cases} \tag{1}$$

with for cell i the remapped quantity A_i, A_i^{lag} on the Lagrangian mesh and with the fluxes through faces or corners dA_{cf}:

$$\begin{cases} dm_{cf} &= \rho_{cf}^{o2} & dVol_{cf} \\ dqu_{cf} &= u_{cf}^{o2} & dm_{cf} \\ dqv_{cf} &= v_{cf}^{o2} & dm_{cf} \\ dmE_{cf} &= \left(e_{cf}^{o2}+k_{cf}^{o2}\right) & dm_{cf} \end{cases} \tag{2}$$

Notice that second order remap is obtained by MUSCL limited linear reconstruction of quantities ρ_{cf}^{o2}, u_{cf}^{o2}, v_{cf}^{o2}, e_{cf}^{o2}, and $k_{cf}^{o2}=((u^2+v^2)/2)_{cf}^{o2}$ at the volume fluxes centers $dVol_{cf}$.

Remark 3.1

We are aware that reconstructing separately ρ and e instead of (ρe) produces a second order error on pressure profiles, but we keep it that way for the sake of simplicity of the description ,and it is a robust choice. The study can be done as well considering the remap of ρ, (ρu), and (ρe) with the same result with definitions $u_{cf}^{o2}=(\rho u)_{cf}^{o2}/\rho_{cf}^{o2}$ and $e_{cf}^{o2}=(\rho e)_{cf}^{o2}/\rho_{cf}^{o2}$.

Let us consider a locally 1D total energy remap with only one mass flux $dm_f>0$ through face f between Lagrangian cells i and $i+1$.

DOI: 10.1002/fld

Considering cell i,

$$\begin{cases} m_i - m_i^{lag} + dm_f = 0 \\ m_i u_i - m_i^{lag} u_i^{lag} + dm_f u_f^{o2} = 0 \\ m_i E_i - m_i^{lag} E_i^{lag} + dm_f E_f^{o2} = 0 \end{cases} \tag{3}$$

with second order reconstruction A_f^{o2} at face f. The remap scheme for total energy in (3) can be developed considering the sum of internal energy and kinetic energy $E_f^{o2} = e_f^{o2} + k_f^{o2}$:

$$m_i e_i - m_i^{lag} e_i^{lag} + dm_f e_f^{o2} = \epsilon_i$$

with

$$\begin{aligned} \epsilon_i &= m_i^{lag} k_i^{lag} - m_i k_i - dm_f k_f^{o2} \\ &= -\frac{dm_f m_i^{lag}}{m_i} \frac{\left(u_i^{lag} - u_f^{o2}\right)^2}{2} - dm_f \left(k_f^{o2} - \frac{(u_f^{o2})^2}{2}\right) \end{aligned} \tag{4}$$

with kinetic energies $k_i^{lag} = (u_i^{lag})^2/2$ and $k_i = (u_i)^2/2$ imposed by the momentum remap.

Considering cell $i+1$,

$$\begin{cases} m_{i+1} - m_{i+1}^{lag} - dm_f = 0 \\ m_{i+1} u_{i+1} - m_{i+1}^{lag} u_{i+1}^{lag} - dm_f u_f^{o2} = 0 \\ m_{i+1} E_{i+1} - m_{i+1}^{lag} E_{i+1}^{lag} - dm_f E_f^{o2} = 0 \end{cases} \tag{5}$$

then the equivalent internal energy remap writes the following:

$$m_{i+1} e_{i+1} - m_{i+1}^{lag} e_{i+1}^{lag} - dm_f e_f^{o2} = \epsilon_{i+1}$$

with

$$\begin{aligned} \epsilon_{i+1} &= m_{i+1}^{lag} k_{i+1}^{lag} - m_{i+1} k_{i+1} + dm_f k_f^{o2} \\ &= \frac{dm_f m_{i+1}^{lag}}{m_{i+1}} \frac{\left(u_{i+1}^{lag} - u_f^{o2}\right)^2}{2} + dm_f \left(k_f^{o2} - \frac{\left(u_f^{o2}\right)^2}{2}\right) \end{aligned} \tag{6}$$

Because we would like an "adiabatic" remap, meaning here that remapped internal energy is not modified by unsigned source terms like ϵ_i and ϵ_{i+1}, we should find k_f^{o2} such that $\epsilon_i \approx 0$ and $\epsilon_{i+1} \approx 0$. Both can obviously not be nullified simultaneously in general, because that would correspond to an internal energy remap which is non conservative in total energy.

Let us see in 1D what are these source terms ϵ_i and ϵ_{i+1} with a classical choice for kinetic energy reconstruction:

$$k_f^{o2} = \frac{\left(u_f^{o2}\right)^2}{2}. \tag{7}$$

This choice leads to the following:

$$\begin{cases} \epsilon_i = -\left(\frac{dm_f m_i^{lag}}{m_i}\right) \frac{\left(u_f^{o2} - u_i^{lag}\right)^2}{2} < 0 \\ \epsilon_{i+1} = \left(\frac{dm_f m_{i+1}^{lag}}{m_{i+1}}\right) \frac{\left(u_{i+1}^{lag} - u_f^{o2}\right)^2}{2} > 0 \end{cases} \tag{8}$$

DOI: 10.1002/fld

Notice that these terms are of opposite signs and are proportional to dm_f, meaning first order because $dm_f = \rho_f A_f u_f \Delta t$. Analysis of Equations (4) and (6) dependency to k_f^{o2} gives a choice that reduces $|\epsilon_i|$ and $|\epsilon_{i+1}|$:

$$k_f^{o2} = \frac{\left(u_f^{o2}\right)^2}{2} - \frac{\left(u_f^{o2} - u^{lag}_{f\ upw}\right)^2}{2} \tag{9}$$

with the donor cell value $u^{lag}_{f\ upw} = u_i^{lag}$ if $dm_f > 0$, else $u^{lag}_{f\ upw} = u_{i+1}^{lag}$.

In our example, $dm_f > 0$, thus, $u^{lag}_{f\ upw} = u_i^{lag}$ and it yields:

$$\begin{cases} \epsilon_i = -\left(\frac{(dm_f)^2}{m_i}\right) \frac{\left(u_f^{o2} - u_i^{lag}\right)^2}{2} < 0 \\ \epsilon_{i+1} = -\left(\frac{(dm_f)^2}{m_{i+1}}\right) \frac{\left(u_{i+1}^{lag} - u_f^{o2}\right)^2}{2} + \left(dm_f\right)\left(\frac{\left(u_{i+1}^{lag} - u_f^{o2}\right)^2}{2} - \frac{\left(u_f^{o2} - u_i^{lag}\right)^2}{2}\right) \end{cases} \tag{10}$$

With this choice, if we define the MUSCL limited linear velocity reconstruction at faces such that

$$u_f^{o2} = u_i^{lag} + (\varphi_f/2)\Delta u_f$$

with $\Delta u_f = (u_{i+1}^{lag} - u_i^{lag})$ and $\varphi_f = \varphi(\theta_f)$ a classical limiter function of local slope ratios, for instance:

- Minmod $\varphi(\theta) = \min(1, \max(0, \theta))$
- VanLeer $\varphi(\theta) = \frac{\theta + |\theta|}{1 + \theta|}$

with here $\theta_f = \frac{u_i^{lag} - u_{i-1}^{lag}}{u_{i+1}^{lag} - u_i^{lag}}$.

It comes as fpllows:

$$\begin{cases} \epsilon_i = -\left(\frac{(dm_f)^2}{m_i}\right) \frac{(\varphi_f/2)^2 \Delta u^2}{2} < 0 \\ \epsilon_{i+1} = -\left(\frac{(dm_f)^2}{m_{i+1}}\right) \frac{(1-\varphi_f/2)^2 \Delta u^2}{2} + \left(dm_f\right) \frac{(1-\varphi_f)\Delta u^2}{2} \end{cases} \tag{11}$$

When the scheme turns first order in space, that is, $\varphi = 0$, thus, $u_f^{o2} = u_i^{lag}$ when for any cell k $u_k^{lag} > 0$, then internal energy is created by the remap because $\epsilon_i = 0$ and $\epsilon_{i+1} \geq 0$. In smooth regions of the flow where u is locally linear and when using, for instance, the Minmod limiter $\varphi(\theta) = \max(0, \min(1, \theta))$, then $\varphi_f = 1$, thus, ϵ_i and ϵ_{i+1} are second order, that is, proportional to $(dm_f)^2$. For more compressive limiters than Minmod, allowing $2 > \varphi > 1$ as Van Leer, first order negative terms can exist in ϵ_{i+1}. However, maximum principle breakings can also occur in an internal energy remap with those limiters when the monotonicity constraint $\varphi \leq 1$ is not fulfilled.

3.2. Result

As an example in Figure 13, let us compute a double rarefaction wave test case. Two states are initially ($\rho = 1$, $u = -2$, $p = 0.4$) at left hand side and ($\rho = 1$, $u = 2$, $p = 0.4$) at right hand side, for a perfect gas of equation $p = (\gamma - 1)\rho e$ with $\gamma = 1.4$. The result is a strong rarefaction at the center, where specific entropy $s = log(p/(\gamma - 1)\rho^\gamma)$ should stay null because there exits only expansion waves in this test. When using the kinetic energy reconstruction (9), the result on entropy (in black) is much better because there is no more zones where it decreases (in red). Moreover, internal energy is kept above the theoretical value, because the profile goes below without correction, which is a good sign for robustness.

DOI: 10.1002/fld

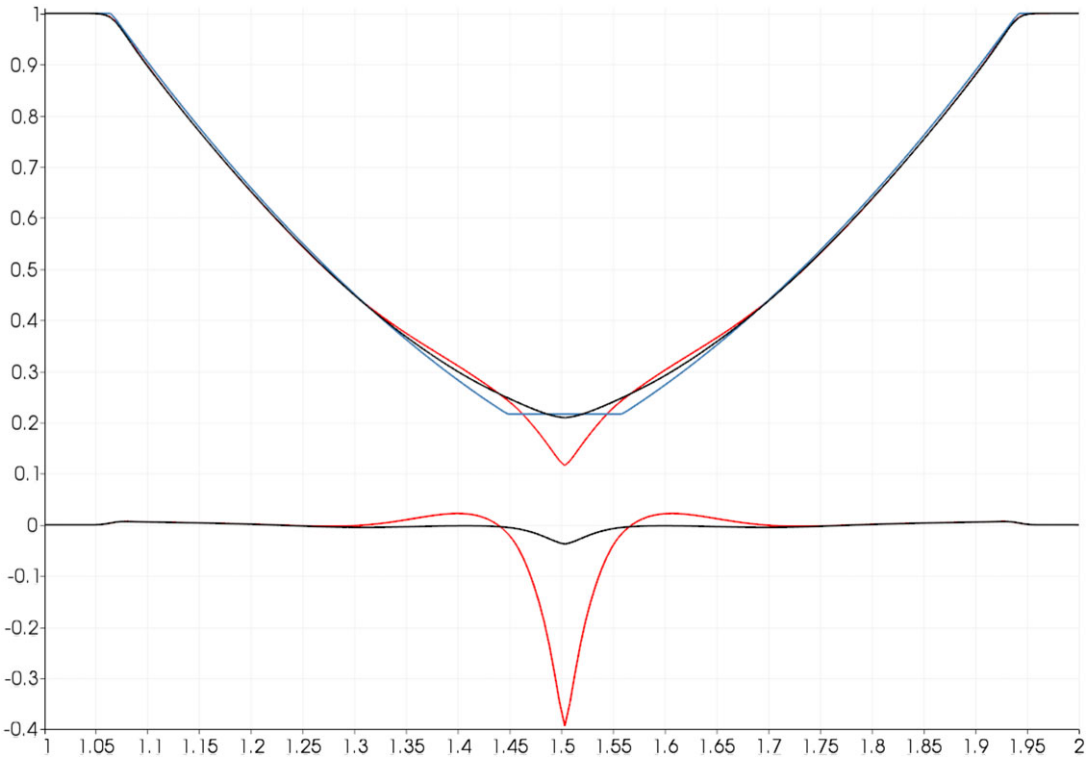

Figure 13. Double rarefaction wave, 201 cells, specific internal energy (above) and specific entropy $s = log(p/(\gamma-1)\rho^{\gamma})$(below), comparison EUCCLHYD + total energy remap, with (black) and without (red) corrected 'k', exact solution for internal energy (blue). Entropy should stay flat for this isentropic flow. One can see the bad behavior of the uncorrected total energy remap in red leading to negative values for entropy. The corrected remap in black shows a good behavior, because entropy increases, and internal energy has a proper behavior compared with the exact solution.

4. CONCLUSION

In this paper, we have described a multi-material conservative Lagrange-remap Eulerian scheme on Cartesian planar orthogonal meshes. The multi-dimensional collocated remap gives very close results compared with the reference AD remap. Even if accuracy is equivalent and not improved on the presented test cases as we could have expect, the direct remap with corner fluxes is more adapted to HPC parallelization, because only one MPI (Message Passing Interface) synchronization is necessary for the remap and each face or corner flux can be computed independently, thus can be distributed to computational cores that share the memory. The whole scheme is conservative and entropic at first order, thus, its convergence properties should be good, but it should be further studied. The test cases show that robustness is good even for violent multi-material flows with stiffened gas equations of state. We also propose a second order remap of total energy that improves the internal energy behavior, that is, entropy behavior. The algorithm parallelization efficiency should be evaluated (scalability), to demonstrate the benefits of a single step direct remap compared with a directional splitting remap with several monodimensional steps. This remap could be extended to cylindrical geometry and 3D with no anticipated difficulties. The extension of this direct remap to general meshes requires a general definition of corner fluxes and a multi-dimensional reconstruction of variables, which could provide a suitable and efficient remap for multi-material ALE.

REFERENCES

1. Després B, Mazeran C. Lagrangian gas dynamics in two dymensions and lagrangian schemes. *Archive for Rational Mechanics and Analysis* 2005; **178**:327–371.

DOI: 10.1002/fld

2. Maire PH, Abgrall R, Breil J, Ovadia J. A cell-centered Lagrangian scheme for two-dimensional compressible flow problems. *SIAM Journal on Scientific Computing* 2007; **29**(4):1781–1824.
3. Burton DE, Carney TC, Morgan NR, Sambasivan SK, Shashkov MJ. A cell-centered Lagrangian Godunov-like method for solid dynamics. *Computers & Fluids* 2013; **83**:33–47.
4. Barlow AJ, Roe PL. A cell centred Lagrangian Godunov scheme for shock hydrodynamics. *Computers & Fluids* 2011; **46**:133–136.
5. Maire PH, Abgrall R, Breil J, Loubere R, Rebourcet B. A nominally second-order cell-centered Lagrangian scheme for simulating elastic-plastic flows on two-dimensional unstructured grids. *Journal of Computational Physics* 2013; **235**:626–665.
6. Maire PH. A high-order cell-centered Lagrangian scheme for compressible fluid flows in two-dimensional cylindrical geometry. *Journal of Computational Physics* 2009; **228**:6882–6915.
7. Breil J, Maire PH. A cell-centered diffusion scheme on two-dimensional unstructured meshes. *Journal of Computational Physics* 2007; **224**:785–823.
8. Galera S, Maire PH, Breil J. A two-dimensional unstructured cell-centered multimaterial ALE scheme using VOF interface reconstruction. *Journal of Computational Physics* 2010; **229**:5755–5787.
9. Lafaurie B, Nardone C, Scardovelli R, Zaleski S, Zanetti G. Modelling merging and fragmentation in multiphase flows with SURFER. *Journal of Computational Physics* 1994; **113**(1):134–147.
10. Youngs DL. Time-dependent multi-material flow with large fluid distortion, in. In *Numerical Methods for Fluid Dynamics, Academic*, Morton KW, Baines MJ (eds).: New York, 1982; 273–285.
11. Rider WJ, Kothe DB. Tracking reconstructing volume. *Journal of Computational Physics* 1998; **141**:112–152.
12. LeVeque RJ. High-resolution conservative algorithms for advection in incompressible flow. *SIAM Journal on Numerical Analysis* 1996; **33**(2):627–665.
13. Carré G, Del Pino S, Després B, Labourasse E. A cell-centered Lagrangian hydrodynamics scheme on general unstructured meshes in arbitrary dimension. *Journal of Computational Physics* 2009; **228**:5160–5183.
14. Haas JF, Sturtevant B. Interaction of weak-shock waves. *Journal of Fluid Mechanics* 1987; **181**:41–76.
15. Burton DE, Morgan NR, Carney TC, Kenamond MA. Reduction of dissipation in Lagrange cell-centered hydrodynamics (CCH) through corner gradient reconstruction (CGR). *Journal of Computational Physics* 2015; **299**:229.
16. Blais B, Braeunig JP, Chauveheid D, Ghidaglia JM, Loubère R. Loubere, Dealing with more than two materials in the FVCF-ENIP method. *European Journal of Mechanics B/Fluids* 2013; **42**:1–9.
17. Maire PH, Nkonga B. Multi-scale Godunov-type method for cell-centered discrete Lagrangian hydrodynamics. *Journal of Computational Physics* 2009; **228**:799–821.
18. Maire PH, Breil J, Galera S. A cell-centred arbitrary Lagrangian-Eulerian (ALE) method. *International Journal for Numerical Methods in Fluids* 2008; **56**(8):1161.

DOI: 10.1002/fld